Published in final edited form as:
Neuron. 2013 April 10; 78(1): 81–93. doi:10.1016/j.neuron.2013.02.011.

Imaging patients with psychosis and a mouse model establishes a spreading pattern of hippocampal dysfunction and implicates glutamate as a pathogenic driver

Scott A. Schobel[1,2,&], **Nashid H. Chaudhury**[2,%], **Usman A. Khan**[3,4], **Beatriz Paniagua**[5,6], **Martin A. Styner**[5,6], **Iris Asllani**[7], **Benjamin P. Inbar**[2], **Cheryl M. Corcoran**[1,2], **Jeffrey A. Lieberman**[1,2], **Holly Moore**[1,2,*], and **Scott A. Small**[3,*]

[1]Department of Psychiatry, Columbia University Medical Center, New York, NY 10032

[2]The New York State Psychiatric Institute, New York NY, 10032

[3]Department of Neurology, Columbia University Medical Center New York, NY 10032

[4]State University of New York (SUNY) Downstate Medical Center Brooklyn, NY 11203

[5]Department of Psychiatry, University of North Carolina at Chapel Hill Chapel Hill, NC 27514

[6]Computer Science, University of North Carolina at Chapel Hill Chapel Hill, NC 27514

[7]Department of Radiology, Columbia University Medical Center

SUMMARY

The hippocampus in schizophrenia is characterized by both hypermetabolism and reduced size. It remains unknown whether these abnormalities are mechanistically linked. Here, in addressing these questions we used MRI tools that can map hippocampal metabolism and structure in patients and mouse models. In at-risk patients, hypermetabolism was found to begin in CA1 and spread to the subiculum after psychosis onset. CA1 hypermetabolism at baseline predicted hippocampal atrophy, which occured during progression to psychosis, most prominently in similar regions. Next, we used ketamine to model conditions of acute psychosis in mice. Acute ketamine reproduced a regional pattern of hippocampal hypermetabolism, while repeated exposure shifted the hippocampus to a hypermetabolic state with concurrent atrophy and pathology in parvalbumin-expressing interneurons. Parallel in vivo experiments using LY379268 and direct measurements of extracellular glutamate showed that glutamate drives both neuroimaging abnormalities. These findings show that hippocampal hypermetabolism leads to atrophy in psychotic disorder and suggest glutamate as a pathogenic driver.

INTRODUCTION

Previous research has demonstrated functional and structural and abnormalities in the hippocampus of patients with schizophrenia and related psychotic disorders. Among the

[*]Co-corresponding authors: sas68@columbia.edu, hm2035@columbia.edu.
[&]Present address: F. Hoffman-La Roche Ltd, Basel, Switzerland 4070
[%]Present address: Yale University School of Medicine, New Haven, CT 06510

most prominent are hypermetabolism and volume reduction of the hippocampus as reflected in neuroimaging studies (Heckers et al., 1998; Kawasaki et al., 1992; Malaspina et al., 2004; Medoff et al., 2001; Molina et al., 2003; Steen et al., 2006).

The hippocampal formation is a complex structure comprised of different subregions extending the posterior-to-anterior extent of the medial temporal lobe to form a neural circuit (Small et al., 2011). Recent neuroimaging studies have shown that the CA1 and subiculum in the anterior body of the hippocampus are differentially affected in schizophrenia, as reflected by volume (Kuhn et al., 2012), shape (Csernansky et al., 1998; Narr et al., 2004), and metabolic measures (Schobel et al., 2009b). The overlap between the anatomical pattern of hippocampal hypermetabolism and apparent atrophy suggests that these neuroimaging abnormalities might have a common pathophysiologic mechanism. However, as these neuroimaging tools have not yet been applied within the same population of subjects, the precise concordance between hypermetabolism and atrophy remains unknown. Furthermore, as it is now understood that schizophrenia is a progressive brain disease (Andreasen et al., 2011), the temporal sequence of these pathologic features remains uncharted.

Accordingly, to map the spatial and temporal pattern of hippocampal metabolism and structure, we longitudinally assessed subjects who fulfilled ‘clinical high-risk’ criteria using magnetic resonance imaging (MRI) methods. Previous studies have shown that about 30% of this enriched group of subjects with prodromal symptoms progress to psychosis (Fusar-Poli et al., 2012). We previously reported that baseline MRI maps of cerebral blood volume (CBV), an established hemodynamic correlate of basal metabolism (Gonzalez et al., 1995; Raichle, 1983), predicts progression to psychosis (Schobel et al., 2009b). In the present study we imaged subjects at baseline and after follow-up periods, using both CBV-fMRI and structural MRI measures. The results show that hippocampal hypermetabolism antedates atrophy and that over time an anatomical concordance emerges between the specific pattern of hypermetabolism and atrophy.

The anatomical concordance of metabolism and structure suggested a common mechanism, and based upon current glutamatergic theories (Lisman et al., 2008; Moghaddam and Javitt, 2012) we hypothesized that elevations in extracellular glutamate might act as a pathogenic driver. This hypothesis was informed, in part, by prior observations in a mouse model deficient in glutamate, developed to understand how alterations in the glutamatergic system relate to schizophrenia-relevant neuroimaging and behavioral phenotypes (Gaisler- Salomon et al., 2009). By fMRI, *reductions* in CBV were observed in the same subregions characterized by hypermetabolism in schizophrenia; moreover this ‘inverse’ neuroimaging phenotype was accompanied by behavioral and neurochemical phenotypes that were in all cases the inverse of what typically characterizes animal models of schizophrenia. These results were interpreted in the context of a growing number of studies suggesting that excess extracellular glutamate may be a contributing factor in psychosis. Systemic administration of Nmethyl-D-aspartate (NMDA) receptor antagonists provides proof of this principal. These agents, induce both positive and negative symptoms of the disease in healthy volunteers (Krystal et al., 1994) and exacerbate psychotic symptoms and cognitive impairments in patients with schizophrenia (Malhotra et al., 1997). Moreover, in experimental animals, NMDA antagonists elevate extracellular glutamate (Moghaddam and Javitt 2012) and induce hypermetabolism in cerebral cortex as detected by CBV-fMRI (Gozzi et al., 2007) at doses that induce behavioral and neurochemical abnormalities homologous with schizophrenia (Bickel and Javitt, 2009; Jentsch and Roth, 1999; Moghaddam et al., 1997; Mouri et al., 2007; Pinault, 2008).

To test the hypothesis that excess glutamate drives hippocampal subregional hypermetabolism and atrophy in psychosis, we used administration of the NMDA antagonist ketamine in mice, where invasive technologies can be deployed to precisely map extracellular glutamate within the hippocampal circuit. First, we used the same MRI tools applied to human patients to show that that ketamine administration in rodents replicated the specific anatomical pattern of hippocampal dysfunction in schizophrenia. We then conducted a series of experiments utilizing an *in vivo* glutamate biosensor method (Hu et al., 1994) in multiple hippocampal subregions to show that ketamine causes a regionally preferential increase in extracellular glutamate, and that a glutamate-reducing agent ameliorates this increase, as well as MRI-detected hippocampal hypermetabolism and atrophy. Finally, we performed post-mortem analyses to determine histopathological correlates of the neuroimaging phenotypes.

RESULTS

Mapping a neuroimaging pattern of hippocampal dysfunction during the emergence of psychosis

Twenty five subjects at clinical high-risk for a psychotic disorder were imaged while experiencing prodromal symptoms, and then 20 were re-imaged at clinical follow-up totaling 80% of the original sample. One patient in the progressor group, and four patients in the non-progressor group were lost to brain imaging follow-up, though no were lost to clinical follow-up. The average follow-up period and interscan interval was 2.4 years. During this time ten of the 25 subjects progressed to psychosis, and fifteen subjects did not develop a psychotic disorder (Supplemental Tables 1 and 2). Subjects were comparable on baseline demographic variables including age (t_{23}=.7, p=.48), sex (Fisher's exact p=1.0), years education (t22=0, p=1) and follow-up interval (t_{18}=.8, p=.76).

Mapping hippocampal CBV—Subjects were imaged at baseline and at follow-up using the steady-state gadolinium-enhanced fMRI technique, as previously described (Moreno et al., 2007). Based on our previous findings (Schobel et al., 2009b) we focused on the anterior aspect of the hippocampal formation. For each subject, mean CBV was measured from the following hippocampal subregions—entorhinal cortex (EC), dentate gyrus (DG), CA3, CA1, and subiculum (SUB). A repeated-measures analysis of variance with subregion (EC, DG, CA3, CA1, and SUB) and side (left, right) as within-subject factors and outcome (progression to psychosis vs. non-progression) as between-subjects factor revealed a subregion by progression to psychosis interaction ($F_{4,18}$=3.1, p=.04); Post-hoc t tests revealed increases in CA1 subfield CBV averaged across sides (t_{23}=2.7, p=.01), and, in particular, increases in left-sided CA1 subfield CBV (t_{23}=3.5, p=.002).

To test for longitudinal changes in CBV from baseline to follow-up, a repeated measures analysis with time (baseline and follow-up) and subregion (EC, DG, CA3, CA1, and SUB) as within-subjects factors and progression status (psychosis vs. not) as a between-subjects factor was used. The multivariate component of the analysis identified a significant subregion by time by group interaction ($F_{4, 13}$=3.5, p=.04). Post-hoc t-tests revealed this interaction to be driven by CBV increases in subiculum from baseline to follow-up bilaterally in the progressor group (t_{18}=3.7, p=.002); increases in CA1 CBV did not change significantly from time 1 to time 2, remaining relatively higher in the progressor group at both baseline (t_{23}=2.7, p=.01) and follow-up (t_{18}=3.1, p=.006). EC, DG and CA3 were not significantly different between groups at baseline or follow-up. Antipsychotic or antidepressant drug exposure had no effect on CBV values in this analysis (Figure 1A).

To confirm that hippocampal hypermetabolism is predictive of psychosis, we entered hippocampal left anterior CA1 CBV into a Cox regression model, controlling for

demographics and follow-up interval, with time to psychosis as the dependent variable. Left anterior CA1 CBV powerfully predicted time to psychosis in the Cox model (Wald (t_1)=8.5, p=.003). We further explored whether brain metabolism or symptoms were more powerful predictors of outcome. Similar to other larger prodromal cohort studies (Cannon et al., 2008), unusual thought content (Wald(t_1)=2.9, p=.09) suspiciousness, (Wald(t_1)=2.9, p=.08) and conceptual disorganization (Wald(t_1)=3.5, p=.06) also predicted time to psychosis at a trend level when entered separately into this model. When behavioral variables were entered together into the predictive model with left anterior CA1 CBV, brain metabolism maintained its predictive strength (Wald(t_1)=8.8, p=.003), whereas behavioral measures were no longer predictive of clinical outcome (all p's >.33), suggesting that left CA1 CBV is a more sensitive predictor of clinical outcome to first episode psychosis than subthreshold psychotic symptoms.

Mapping hippocampal structure—In the same subjects, MRI was used to map hippocampal structure and generate measures of hippocampal volume and hippocampal shape as previously described (Schobel et al., 2009a; Styner, 2003). At the initial assessment, to test for baseline differences in hippocampal volume, a repeated-measures analysis of variance with side (left, right) as within-subject factors and outcome (progression to psychosis vs. non-progression) as between-subjects factor revealed no main effect of progression status ($F_{1,22}$=.96, p=.36) and no side-by-conversion interaction ($F_{1,22}$=1.1, p=.30). To test for hippocampal atrophy over time, a repeated measures analysis with time (baseline and follow-up) and hippocampal volume as within-subjects factors and progression status (psychosis vs. not) as a between-subjects factor, controlling for baseline hippocampal volume, revealed a group by time interaction ($F_{1,16}$= 17.6, p=.001), in which the hippocampal volume of progressors to psychosis declined bilaterally (t_{18}=4.6, p<.001) (Figure 1B). Antipsychotic or antidepressant exposure had no effect on hippocampal volumes at either time 1 or time 2 between groups.

To map the site of within the hippocampus where atrophy where occurred and whether it was localized to a specific hippocampal subregion, morphological analysis of the longitudinal assessments was performed (Figure 1C, 1D). Compared to non-progressors, progressors had volume loss localized to the CA1 and subiculum subregions, which were most prominent in the anterior body of the left hippocampus (Figure 1C, 1D).

The relationship between hippocampal CBV and atrophy—To investigate the spatiotemporal relationship between hippocampal CBV acquired at baseline and subsequent hippocampal structural changes, we first visualized the left hippocampal morphometric shape result (Figure 1C) in a magnified fashion, focusing upon the extent of the long axis of the hippocampal body containing the left CA1 subfield (Figure 2A). We then generated baseline CA1 CBV values in subjects along the extent of the same area of the long axis of the hippocampal body. CBV values from the posterior to anterior extent of the hippocampal body were entered into a single multivariate analysis of variance with hippocampal long axis CBV as within-subjects factors and progression status (psychosis vs. not) as a between-subjects factor, controlling for demographics (both left and right sides included in the analysis; Figure 2B shows an example of left long axis CA1 CBV of the hippocampal body from posterior to anterior in an individual subject). CBV increases at baseline were localized to the two most anterior slices of the left body of the hippocampus (F_1=10.8, p=.002; F_1=3.6, p=.07; respectively) (Figure 2C). Taken together, the results show an anatomical overlap between left anterior hippocampal body CA1 CBV acquired at baseline and the most significant morphologic shape change across the transition to psychosis found in left anterior hippocampal body CA1. To confirm this spatiotemporal relationship, we tested the association of baseline hippocampal CBV along the long axis to subsequent hippocampal volume change. Higher baseline CBV values in left CA1 in the anterior hippocampal body

predicted subsequent hippocampal atrophy at follow-up (beta=−.63, t=2.53, p=.03), an association not found in the posterior body (beta=−.17, t=.76, p=.45) and mid-body CA1 subfields (beta=−.3, t=1.2, p=.24) (Figure 2D). Moreover, this association was specifically found between elevated baseline left anterior CBV values and subsequent left hippocampal volume decrease (beta .58, t=2.9, p=.01).

Mapping a neuroimaging pattern of hippocampal dysfunction induced by acute ketamine administration in mice

Male C57B6 mice aged 50–70 days postnatal (n=9 per group), an age range analogous to young adulthood in the human (Laviola et al., 2003), were used for this experiment. While the mice were stably anesthetized, we administered an acute ketamine (30mg/kg) or saline challenge; CBV was then measured within subregions (EC, DG, CA3, CA1, SUB) of the ventral hippocampal body at 16, 32, and 48 min post-challenge using previously described CBV-fMRI imaging methods (Moreno et al., 2006). A mixed ANOVA showed an interaction between drug challenge and post-injection time, with ketamine-induced increases in CBV observed in CA1 ($F_{4,13}$=4.1, p=.02) (Figure 3A) and subiculum ($F_{4,13}$=3.8, p=.03) subregions (Figure 3B). Planned pairwise comparisons showed significant increases (relative to pre-injection baseline) at 16 min (CA1: t_8=4.3, p=.003; SUB: t_8=4.8, p=.001) which persisted at a trend level at 32 min (CA1: t_8=1.9, p=.09;SUB t_8=2.1, p=.07) (Figure 3 A–B) For both CA1 and subiculum, saline injection produced no significant increases in CBV relative to pre-injection baseline. Moreover, there were no statistically significant effects of ketamine (relative to baseline or saline) within EC, DG or CA3 (Figure 3 C–E).

Mapping a neuroimaging pattern of hippocampal dysfunction after repeated ketamine administration in mice

Mapping hippocampal CBV—To model episodic neurochemical conditions that may precipitate psychosis, we exposed C57B6 male mice ages 35–45 days (n=6–10 per group), to three times weekly exposure to ketamine (8mg/kg, 16mg/kg, and 32mg/kg dose groups) or saline for one month (total 12 doses per group) (Supplemental Figure 1). The age range is considered to be analogous to the period from mid-adolescence through young adulthood in human (Laviola et al., 2003), during which time the risk for psychosis rises sharply in males (Paus et al., 2008). At the end of the 1-month treatment (at age 65–75 days), following a 48- to 72-hour washout period, we imaged basal CBV. An ANOVA revealed a main effect of drug dose on basal hippocampal CBV at one month ($F_{3,28}$=3.3, p=.035); planned pair-wise comparisons of each ketamine dose group to saline showed that repeated ketamine led, with an inverse “U” shaped dose function, to an increase in basal-state CBV preferentially in the CA1 subfield (Figure 4A). Specifically, relative to saline administration, exposure to intermittent ketamine 8mg/kg resulted in increases in basal CBV in the CA1 subfield (t_3=4.3, p=.02); exposure to the 16/mg dose resulted in increases in the CA1 subfield (t_9=2.3, p=.05) as well as trends for increases in the CA3 subfield (t_9=1.8, p=.08) and subiculum (t_9=1.9, p=.09). Exposure to the 32mg/kg dose resulted in less robust increases in basal CBV across subregions (all p’s>.2).

Mapping hippocampal structure—Structural imaging was performed on the same mice used in the repeated ketamine study at baseline (at age 35–45 days, n=6–10 per group) and following the 1-month treatment (at age 65–75 days). For this study, for total forebrain and total hippocampal volume were determined using structural T2-weighted horizontal MRI images (24 slices, rostral to dorsal, 86μM in plane resolution, 500 μM slice thickness). Not surprisingly, during acute exposure there was no change in hippocampal volume ($F_{3, 26}$=.64, p=.59). We next compared hippocampal volume change over the one month amongst the four groups, controlling for whole brain volume. Results revealed a main effect of group on hippocampal volume change ($F_{3, 26}$=12.9, p<.001). Post-hoc tests showed the 16mg/kg

(t_{18}=5.3, p<.001) and 32mg/kg (t_{14}=3.8, p=.002) groups had a relative loss of volume; specifically mice treated at these doses showed no growth or a loss of hippocampal volume over one month relative to the saline-exposed group, which showed increases in volume over the month (Figure 4B). To map the site of negative hippocampal growth, morphological analysis of the longitudinal assessments was performed. Compared to the saline group, mice exposed to 16mg/kg had volume loss localized to the ventral portion of hippocampal body (Figure 4C).

Gross hippocampal structure was also assessed post-mortem in fixed, immunostained tissue in a subset of mice from this study and the related experiment assessing the effect of cotreatment with LY379268 (see below). For these studies, we systematically sampled coronal sections through the body of the hippocampus, calculating average cross-sectional area of blocks matched across groups for location within hippocampus. Guided by the imaging findings, we divided the body into a rostrodorsal portion (1.0 to 2.4 mm posterior to Bregma; rostral to the emergence of the ventral hippocampus) and caudoventral portion (2.5 to 4.0 mm posterior to Bregma, including ventral hippocampus). An omnibus analysis including the three repeated drug treatment groups (saline-only control, saline co-treatment with ketamine [16 mg/kg], and LY379268 [10 mg/kg] co-treatment with ketamine [16 mg/kg]) showed a significant interaction between drug condition and position within the hippocampus ($F_{2,14} = 4.7$, $p < 0.05$). Planned comparisons between the saline control and repeated ketamine groups revealed that while there was no difference between drug groups for the rostrodorsal hippocampus ($t_8 = 0.26$, 1-tailed $p > 0.4$), the caudoventral hippocampus was reduced in size in the repeated ketamineexposed mice relative to saline ($t_8 = 1.93$, $p < .05$) (Figure 4D).

Excess glutamate mediates the psychosis-associated neuroimaging pattern of hippocampal dysfunction

To determine whether extracellular glutamate mediated the acute effect of ketamine on hippocampal CBV, ketamine 30mg/kg or saline was administered via an i.p. catheter under the same experimental conditions used in the acute ketamine CBV experiments above, and the extracellular glutamate response was recorded in specific hippocampal subregions *in vivo* following implantation of an amperometric glutamate biosensor (Hu et al., 1994). An ANOVA showed a significant ketamine-evoked increase in hippocampal glutamate ($F_{3,24}$=4.6, p=.01); planned comparisons showed increases in the CA1 (t_{11}=2.4, p=.03) and SUB (t_{10}=2.5, p=.03) relative to the EC which showed no increase following ketamine (Figure 5A, 5B).

To determine whether increases in extracellular glutamate were necessary for ketamineevoked hippocampal hypermetabolism to occur, we pre-treated mice with LY379268(10mg/kg), a drug which reduces neuronal glutamate release through activation of presynaptic mGlur2/3 receptors (Lorrain et al., 2003; Monn et al., 1999) Mice were pre-treated for five days with LY379268 or saline prior to recording the extracellular glutamate response or CBV response to acute ketamine challenge 30mg/kg. An ANOVA revealed that L379268 blocked the ketamine-evoked glutamate elevation in CA1/SUB ($F_{1,11}$=5.5, p=.04) (Figure 5C). At this glutamate-suppressing dose, LY379268 also prevented ketamine-induced increases in CA1/SUB CBV (overall $F_{2,27}$=21.7, p<.001); planned comparisons of LY379268 to SAL pretreatment (p<.001) (Figure 5D).

To determine whether glutamate mediated the induction of the hypermetabolic state and relative volume loss observed with repeated intermittent ketamine exposure, mice were administered either saline or LY379268(10mg/kg) one hour prior to receiving each ketamine (16mg/kg) treatment, totaling 12 (3 weekly) co-treatments over one month. Prior to endpoint CBV and structural hippocampal imaging, all animals were withdrawn from treatment for 48

hours. LY739268 prevented ketamine-induced basal increases in CBV throughout the trisynaptic circuit and subiculum (DG $F_{1,17}$=7.0, p=.01; CA3 $F_{1,17}$=5.2, p=.04; CA1 $F_{1,17}$=4.3, p=.05; SUB $F_{1,17}$=6.1, p=.03; (Figure 6A). At this basal hypermetabolism-suppressing dose, LY379268 also prevented the repeated ketamine-induced hippocampal volume decrease over the one month exposure ($F_{1,17}$=11.7, p=.003) (Figure 6B). Additional morphometric analyses revealed that the region showing the most consistent relative protection overlapped with midbody CA1 and subiculum (Figure 6C). This was consistent with the post-mortem analysis (performed as described above) which showed an effect of LY379268 co-treatment on hippocampal structure following repeated ketamine (Figure 6D). Specifically, while there were no group differences observed in the rostrodorsal hippocampus, the size of the caudoventral hippocampus was larger in repeated ketamine-treated mice receiving LY379268 co-treatment than mice co-treated with saline (t12 = 2.1, 1-tailed p<.05).

GABAergic interneuronal markers are linked to the neuroimaging pattern of hippocampal dysfunction

To further investigate circuit mediators of the above effects of repeated ketamine, we quantified the density of the parvalbumin-positive (PV+) subpopulation of GABAergic interneurons in the CA fields of three groups from the longitudinal treatment studies (saline/saline [saline control], saline/ketamine16mg/kg, LY37926810mg/kg/ketamine 16mg/kg). A general linear model showed significant differences in PV+ cell density across treatment groups (Wald Chi-Square [df=2] = 8.1, p <.05). Pairwise comparisons (Wald) revealed that repeated ketamine exposure (saline/ketamine16mg/kg group) led to significant decreases in PV+ cell density relative to the saline control group (p <.01) (Figure 7A). PV+ cell density in the LY379268 was intermediate, not differing significantly from either saline control or the saline/ketamine group (Figure 7A). Interestingly, there was a strong trend across the three groups for decreases in PV+ cell density (relative to the mean saline control value) to correlate with increases in basal CA1 CBV observed after repeated ketamine exposure (r=.49, p=.06) (Figure 7B). In turn, this abnormal increase in basal CA1 CBV was significantly related to hippocampal volume loss (r=.57, p=.006) (Figure 7C).

DISCUSSION

Schizophrenia characteristically has a gradual onset beginning with a prodromal stage and culminating with psychotic symptoms. Neuroimaging studies have demonstrated pathological involvement of the hippocampal formation in schizophrenia with structural and functional imaging techniques. These findings pose questions about the fundamental relationship between hippocampal metabolism and structure during the onset and course of schizophrenia. Our longitudinal study of prodromal patients revealed a spatiotemporal pattern of hippocampal dysfunction that progresses in the transition from prodromal symptoms to psychosis. During prodromal pre-psychotic stages hypermetabolism occurs preferentially in the CA1 subregion of the hippocampus in the absence of structural differences. As patients progressed to syndromal psychosis, hypermetabolism spread from CA1 to the subiculum and, importantly, hippocampal volume reduction became evident. A precise spatial concordance was observed between the anatomical pattern of hypermetabolism and atrophy, occurring in the left CA1 and subiculum in the anterior hippocampal body.

This anatomical concordance suggested a common upstream mechanism, so informed by previous studies, we used the NMDA antagonist model of psychosis to test the hypothesis that an elevation in glutamate acts a pathogenic driver. Acute systemic administration of NMDA antagonists such as ketamine and phencyclidine recapitulate many of the features of schizophrenia in humans, and in experimental animals elevates extracellular glutamate at

doses that produce schizophrenia-relevant changes in behavior (Krystal et al., 1994; Moghaddam and Javitt, 2012). Moreover, chronic or repeated exposure to NMDA antagonists produces schizophrenia-relevant cognitive deficits (Jentsch and Roth, 1999) and is associated with cortical gray matter loss in humans (Liao et al., 2011). Previous studies, however, have not mapped ketamine's effect on glutamate levels within the hippocampal circuit. Here, acute ketamine administration produced a gradient of hippocampal hypermetabolism comparable to that observed in the psychosis-stage of schizophrenia. Moreover, chronic administration of ketamine for one month caused a shift in the state of the hippocampus to hypermetabolism, atrophy, and down-regulation of PV+ interneurons, all of which match the anatomical pattern of hippocampal dysfunction observed in patients.

We tested the hypothesis that increases in extracellular glutamate are required to produce these neuroimaging phenotypes in three experiments in the rodent model: First, we found that ketamine-evoked increases in extracellular glutamate mirrored the evoked fMRI pattern, with preferential changes found in the CA1 subfield and subiculum subregion. Second, we established a mechanistic link by showing that pre-treatment with a glutamate mGluR 2/3 agonist known to inhibit glutamate release blocked the ability of ketamine to evoke excess extracellular glutamate *and* increases in CBV. Third, when studied longitudinally, co-treatment with the glutamate release-limiting drug protected against the effects of repeated ketamine on the PV+ interneurons and prevented the associated shift to basal hypermetabolism and hippocampal atrophy. Notably CA1 and subicular subfields in the hippocampal body were most affected with an overall anatomical pattern homologous with that found for progression to psychosis in the human study.

The mGluR 2/3 agonist was an optimal choice to provide this mechanistic link because of its selectivity in limiting glutamate efflux, and its ability to block the behavioral and cognitive abnormalities produced by psychotomimetic drugs (Cartmell et al., 1999; Imre et al., 2006; Krystal et al., 2005; Moghaddam and Adams, 1998). A range of studies now support the hypothesis that glutamate metabolism and neurotransmission play a critical role in driving the cognitive and behavioral disturbances of psychosis (Moghaddam and Javitt, 2012). In the context of systemic NMDA receptor hypofunction, the condition modeled here, NMDA receptor blockade has been shown in neocortex to increase glutamate efflux (Greene, 2001; Moghaddam and Javitt, 2012) thereby increasing metabolic demand and blood flow (Douglas L. Rothman, 2002; Pellerin and Magistretti, 1994). A similar cascade is likely to operate in the hippocampus. Differential regional vulnerability of NMDA receptor blockade may be mediated at a molecular level by the relatively high density of NMDA and AMPA receptors in CA1 relative to other hippocampal subregions (Coultrap et al., 2005). AMPA receptors in particular may play an important role in the consequent synaptic and hemodynamic state (Moghaddam et al., 1997).

The effect of repeated ketamine on PV+ GABAergic interneurons observed here is consistent with previous studies showing that NMDA antagonists lead to metabolic stress, morphologic changes, and down-regulation of PV expression in cortical neurons (Behrens et al., 2007; c.f. Benneyworth et al., 2011; Keilhoff et al., 2004; Vutskits et al., 2007). Further research is needed to relate our results to postmortem findings in schizophrenia, which have shown abnormalities in hippocampal GABAergic interneurons (Heckers and Konradi, 2010), as well as defects in AMPA-kainate and NMDA receptors (Gao et al., 2000; Harrison, 2004; Law and Deakin, 2001). While our findings do not speak to whether acute NMDA blockade on GABAergic interneurons induces a hyperglutamatergic state (see models in Greene, 2001; Lisman et al., 2008; Moghaddam and Javitt, 2012), they provide support for a complementary model: that chronic down-regulation of function in these interneurons caused by a 'toxic' process modeled by repeated episodes of NMDA receptor hypofunction may contribute to the hypermetabolic state observed in early psychosis.

The current study supports the hypothesis that downregulation of hippocampal interneurons may have significant feed-forward excitation of the hippocampal trisynaptic circuit as originally hypothesized by Benes (Benes, 1999). Subsequent elevations in extracellular glutamate may drive further hypermetabolism, progressive interneuronal pathology, and eventual atrophy in the CA1 and subiculum. Consistent with this hypothesis, recent *in vivo* studies using magnetic resonance spectroscopy (MRS) suggest that elevations in glutamate might be characteristic of incipient psychosis in schizophrenia and associated with emergent psychotic symptoms in healthy comparison subjects receiving acute ketamine challenge (de la Fuente-Sandoval et al.; Stone et al., 2012). Currently, however, MRS does not possess sufficient spatial resolution to measure glutamate in individual hippocampal subregions.

In addition to clarifying mechanisms of disease, the results of our study have several clinical implications. CA1 hypermetabolism may be a possible state-specific biomarker of prodromal and early psychotic disorders. As with other progressive disorders of the brain, such as Alzheimer's disease for example, early detection during prodromal stages, when the disease is restricted to relatively confined areas of the brain, has emerged as an important goal for improving therapeutic efficacy. By showing that hypermetabolism occurs before atrophy, our results reinforce this concept, because reversing functional defects are likely easier before the loss of brain tissue. Moreover, our results demonstrate that regulating excess extracellular glutamate and reducing abnormal hippocampal hypermetabolism is protective of hippocampal volume, one of the first and foremost regions to show volumetric loss in schizophrenia (Steen et al., 2006).

Because the glutamate-driven metabolic and structural imaging phenotypes identified in the current study are associated with the emergence of psychosis, we hypothesize that regulating glutamate may be particularly effective during early stages of schizophrenia, a factor not yet considered in recent clinical trials. Notably, glutamate-reducing agents include approved drugs such as lamotrigine or gabapentin, as well as the experimental compound LY404309. It is possible, therefore, to design a study in subjects at clinical high risk for psychotic disorders to test whether glutamate-regulating drugs can normalize hippocampal hypermetabolism, protect hippocampal volume, and prevent progression to threshold psychotic disorder from prodromal stages of disease.

EXPERIMENTAL PROCEDURES

HUMAN STUDIES

Subjects and clinical assessment—Eligibility for study participation and prodromal symptom severity were ascertained using the Structured Interview for Prodromal Syndromes and Scale of Prodromal Symptoms (SIPS/SOPS)(Miller et al., 2003) as previously described(Schobel et al., 2009b). Participants were assessed quarterly for conversion to psychosis using the SOPS, and its Presence of Psychosis (POPS) criteria (Miller et al., 2003). All aspects of the study including clinical assessment and imaging protocols were approved through Columbia University's IRB and the New York State Psychiatric Institute. Written informed consent for subjects over age 18 years or written child assent with written parental consent for subjects under 18 years was obtained after complete description of the study procedures.

Hippocampal cerebral blood volume—As previously reviewed, the use of the contrast agent gadolinium to map cerebral blood volume (CBV) with MRI is a basal state functional imaging approach that provides high spatial resolution (Lin et al., 1999). Cerebral blood volume maps were generated according to methodology as previously described on a Philips 1.5 T scanner (Moreno et al., 2007). Post-gadolinium enhanced images were aligned to pre-gadolinium images in SPM5. Subtracted images (Post minus pre) were then divided by the

contrast-induced difference in signal measured from the superior sagittal sinus (average value of sagittal sinus used in calculation). An investigator blind to subject grouping performed all imaging processing. Of note, all eighteen of the original clinical high-risk participants that were a part of the baseline sample described in Schobel et al 2009 were included in the present manuscript, with n=7 additional cases ascertained at baseline and follow-up, to bring the study to a total n=25 baseline cases and n=20 completing the longitudinal follow-up. All imaging cases were reanalyzed by a single blinded rater for the present manuscript. Strict anatomic criteria for hippocampal subregions along the hippocampal long axis were used to identify brain subregions as previously described (Schobel et al., 2009b).

Hippocampal structure and morphometry—Hippocampal volumes were segmented from the pre-contrast T1 weighted images as previously described using ITK-SNAP (Schobel et al., 2009a; Yushkevich et al., 2006). After validation, these segmented volumes were preprocessed and smoothed (Morey et al., 2009). Point-based models were obtained via spherical parameterizations, and subsequent SPHARM-PDM representation. For more detail of the 3D hippocampal shape representation, please refer to (Styner et al., 2003; Styner, 2003). Statistical analysis was carried out on the aforementioned point-based models as described below.

Statistical Analysis—The statistical models used to analyze the data for clinical studies are found in Supplemental Experimental Procedures.

RODENT STUDIES

Subjects—A total of eighty-eight C57/BL6 (Taconic biosciences) male mice aged 50–70 days were used for the acute ketamine experiment. For the longitudinal study, we used forty-two C57/BL6 mice that were (Taconic, Germantown, NY) aged 35–45 days at the beginning of treatment, and imaged and processed for histology at 65–75 days. All animals were housed 5 to a cage in a vivarium maintained on a 12 hr light/dark cycle. Experiments took place during the light portion of the cycle, and food and water were available ad libitum. All procedures were approved by the Columbia University and New York State Psychiatric Institute Institutional Animal Care and Use Committees.

Drug study design—Ketamine (VedCo, St. Joseph, MO; 100 mg/kg concentration) was diluted to 0.8–3.2 mg/ml and injected at a volume of 10 ml/kg body weight. It was chosen on the basis of its psychotomimetic properties and wider use in (and thus translatability to) humans than other NMDA antagonists. LY379268 (Tocris, Ellisville, MO) was chosen on the basis of its function as an agonist at presynaptic glutamate metabotropic 2/3 receptors and ability to inhibit synaptic glutamate release (Lorrain et al., 2003; Moghaddam and Javitt, 2012; Monn et al., 1999). For acute experiments, ketamine (30mg/kg) or saline challenge was administered after baseline measurement of CBV or extracellular glutamate. For acute drug pre-treatment studies, LY379268 (10mg/kg) vs. saline was administered intraperitoneally (i.p.) once per day for five days prior to measurement of hippocampal CBV or extracellular glutamate. For longitudinal study of intermittent repeated ketamine exposure, mice were treated 3 times per week with saline (10 ml/kg, s.c.) or ketamine (8, 16 or 32 mg/kg, s.c.). For the drug co-treatment longitudinal experiment, animals were administered LY379268 (10 mg/kg, s.c.) 30 minutes prior to each ketamine treatment (16mg/kg, s.c) three times per week for one month. Following the month of treatment, mice were imaged in the drug-free condition after a 48-hr drug washout period.

Hippocampal cerebral blood volume—High-resolution rodent CBV maps (86 μm) were generated as previously described (Moreno et al., 2006; Moreno et al., 2007). After

baseline CBV values were established, mice received either saline or ketamine as described above and three 16-min post-challenge image sequences were obtained.

Hippocampal structure and morphometry—MRI volumes of C57B6 male mice from each group were quantified at baseline (ages 35–45 days, n=6–10 per group) and at follow-up (ages 65–75 days) for total forebrain and total hippocampal volume using structural T-2 weighted horizontal MRI images (24 slices, rostral to dorsal, 86μM in plane resolution, 500 μM slice thickness). Volumes were calculated by using a region-of-interest technique from dorsal to rostral at the first appearance of cortex and hippocampus, respectively, following the external boundary of mouse cortical mantle and hippocampus proper excluding entorhinal cortex (Figure 4C). Rodent morphometry was conducted within a voxel-based framework as described in Sawiak et al (Sawiak et al., 2009). Briefly, a unified segmentation approach was implemented in SPM5 (Wellcome Department of Clinical Neurology, London; http://www.fil.ion.ucl.ac.uk). Affine registered images were transformed to atlas space and assigned a grey matter (GM) probability distribution modulated by the Jacobian determinant of the transformation. Manually segmented hippocampal ROIs were used to conduct small volume correction in statistical analyses. Statistical analysis was performed in a factorial framework implemented in SPM5, with treatment group as the between subject factor and time as within subject factor. Small-volume correction was applied using the hippocampal ROI generated above. Family-wise error (FEW) multiple-comparison correction was applied to all statistical tests with a corrected height threshold of p=.05. Surface renderings of whole-brain and hippocampus ROIs were generated in 3D Slicer (www.slicer.org) using a volume ray casting rendering equation. Maximum intensity projections of T- and F- statistic maps were rendered and overlayed onto the ROI isosurfaces using the volume render module in 3D Slicer.

Measurement of extracellular glutamate—The glutamate biosensor (model 7004, Pinnacle Technologies; Lawrence, KS) was established to be sensitive to micromolar concentrations of glutamate, able to detect rapid changes in extracellular glutamate efflux (<0.5sec response), selective for glutamate, and sufficiently small (130 μM dimension sensing probe) to selectively measure changes within hippocampal subregions (see Hu et al., 1994). On the morning of the experiment, glutamate biosensors were calibrated against glutamic acid using a 3-step concentration curve applied over three minutes. The selectivity of the biosensor response was then tested by administration of 125mM of ascorbic acid and tracing observed over an additional three minutes. After pre-calibration, the biosensors were rinsed in ultra-pure H_2O and then immediately implanted via the arm of the stereotax for in-vivo recording. Sensitivity of the biosensor response (at least 3nA per 10 μM glutamic acid), stability of the response, as well as a non-response to ascorbic acid were required for the biosensor to be inserted for *in vivo* experiments.

Mice were anesthetized with chloral hydrate (400mg/kg) and placed in a stereotax with heating pad post-induction, at which time a 0.6mm i.p. catheter for drug delivery was inserted. Calibrated biosensors were then directly inserted into the ventral hippocampus and connected to the potentiostat for in-vivo recording. Following baseline stabilization of extracellular glutamate signal over one hour, ketamine 30mg/kg or saline was administered via the i.p. catheter and extracellular glutamate response recorded from each hippocampal subregion location over the following 30 minutes (Bregma coordinates EC A-P 4.7, M-L 3.0, D-V 4.0; Dentate Gyrus A-P 3.4, M-L 2.7, D-V 3.8; CA1 subfield A-P 3.5, M-L 3.25, D-V 4.2; Subiculum A-P 3.9, M-L 3.25, D-V 4.2.) Post-experiment, animals were removed from the stereotax, overdosed with chloral hydrate and euthanized by cervical dislocation. Brains were post-fixed in paraformaldehyde (4%), cryoprotected, cryosectioned, thaw mounted, dried, stained with a mixture of cresyl violet and neutral red, dehydrated/defatted

and cover-slipped. Probe placements were verified according to the atlas of (Paxinos and Franklin, 2001) (Supplemental Figure 2).

Histology and estimation of PV+ cell counts and hippocampal cross-sectional area—In a subset of the mice used for the longitudinal study, brains were fixed via transcardial perfusion of buffered saline followed by buffered 4% paraformaldehyde. The brains were then sectioned with a vibratome or cryoprotected and cryosectioned. Coronal 40 micron-thick sections through hippocampus, from the anterior pole to through the posterior extent of the CA fields (approximately 4.3 mm posterior to Bregma). The starting point for sectioning was randomly determined then sections were collected systematically (section interval of either 3 or 4). For some brains post-fixed for more than a few weeks, antigen was retrieved by heating in a 10 mM citrate buffer (pH 8.5, temperature 80 deg C). Parvalbumin was revealed with standard immunohistochemical methods using a monoclonal anti-parvalbumin antibody (PV 235 mouse IgG1, Swant, Marly, Switzerland, dilution 1:800) and a rhodamine anti-mouse secondary (Abcam, Cambridge, MA; dilution 1:200). Following mounting and drying, sections were cover-slipped with an anti-fading medium.

To control for variations in the quality of histology and section preservation, modified stereologically-based methods were used to determine PV+ cell density and average cross-sectional area of the body of the hippocampus. PV+ cells were identified by their relatively large soma lying with strata sub-pyramidale, pyramidale and oriens and the ‘baskets’ frequently formed buy their processes around pyramidal cell soma. In sections between 1.0 to 4.0 posterior to Bregma PV+ cell density was quantified using combined optical fractionator and Cavaleri estimation methods. To estimate changes in hippocampal size following repeated drug treatment, cross-sectional area was calculated using the Cavaleri estimation method for each section used for PV+ cell quantification. For each brain, these sections were aligned according to Paxinos & Franklin (2001) and the average cross-section area for the rostrodorsal body (1.0 to 2.4 posterior to Bregma) and caudoventral body (2.5 to 4.0 mm posterior to Bregma) of the hippocampus were calculated for each brain.

Statistical Analyses—The statistical models used to analyze the data for rodent studies are found in Supplemental Experimental Procedures.

Supplementary Material

Refer to Web version on PubMed Central for supplementary material.

Acknowledgments

This research was supported by The Brain and Behavior Research Fund Young Investigator Grant (http://www.bbrfoundation.org) (S. Schobel); The National Center for Advancing Translational Sciences, NIH, through Grant Number UL1 TR000040, formerly the National Center for Research Resources, Grant Number UL1 RR024156 (S. Schobel); NIMH K23MH090563 (S. Schobel), The Broitman Foundation (S. Small), 1R01MH093398-01 (S. Small), NIMH K23MH066279 (C. Corcoran), The Sidney R. Baer, Jr. Foundation and P50 MH086385 (H. Moore), and the New York State Office of Mental Hygiene. We would like to thank Kenneth Hess and Sara Steinfeld for excellent training and technical assistance on the rodent studies, Elyssa Brent for technical assistance in MR image processing, and Ahmed Gilani and John Wisener for technical assistance with histology experiments. The content is solely the responsibility of the authors and does not necessarily represent the official views of the NIH.

REFERENCES

Andreasen NC, Nopoulos P, Magnotta V, Pierson R, Ziebell S, Ho BC. Progressive brain change in schizophrenia: a prospective longitudinal study of first-episode schizophrenia. Biological psychiatry. 2011; 70:672–679. [PubMed: 21784414]

Behrens MM, Ali SS, Dao DN, Lucero J, Shekhtman G, Quick KL, Dugan LL. Ketamine-induced loss of phenotype of fast-spiking interneurons is mediated by NADPH-oxidase. Science. 2007; 318:1645–1647. [PubMed: 18063801]

Benes FM. Evidence for altered trisynaptic circuitry in schizophrenic hippocampus. Biological psychiatry. 1999; 46:589–599. [PubMed: 10472413]

Benneyworth MA, Roseman AS, Basu AC, Coyle JT. Failure of NMDA receptor hypofunction to induce a pathological reduction in PV-positive GABAergic cell markers. Neuroscience Letters. 2011; 488:267–271. [PubMed: 21094213]

Bickel S, Javitt DC. Neurophysiological and neurochemical animal models of schizophrenia: Focus on glutamate. Behavioural Brain Research. 2009; 204:352–362. [PubMed: 19433116]

Cannon TD, Cadenhead K, Cornblatt B, Woods SW, Addington J, Walker E, Seidman LJ, Perkins D, Tsuang M, McGlashan T, et al. Prediction of psychosis in youth at high clinical risk: a multisite longitudinal study in North America. Arch Gen Psychiatry. 2008; 65:28–37. [see comment]. [PubMed: 18180426]

Cartmell J, Monn JA, Schoepp DD. The metabotropic glutamate 2/3 receptor agonists LY354740 and LY379268 selectively attenuate phencyclidine versus d-amphetamine motor behaviors in rats. J Pharmacol Exp Ther. 1999; 291:161–170. [PubMed: 10490900]

Coultrap SJ, Nixon KM, Alvestad RM, Valenzuela CF, Browning MD. Differential expression of NMDA receptor subunits and splice variants among the CA1, CA3 and dentate gyrus of the adult rat. Brain Res Mol Brain Res. 2005; 135:104–111. [PubMed: 15857673]

Csernansky JG, Joshi S, Wang L, Haller JW, Gado M, Miller JP, Grenander U, Miller MI. Hippocampal morphometry in schizophrenia by high dimensional brain mapping. Proceedings of the National Academy of Sciences of the United States of America. 1998; 95:11406–11411. [PubMed: 9736749]

de la Fuente-Sandoval C, Leon-Ortiz P, Favila R, Stephano S, Mamo D, Ramirez-Bermudez J, Graff-Guerrero A. Higher levels of glutamate in the associative-striatum of subjects with prodromal symptoms of schizophrenia and patients with first-episode psychosis. Neuropsychopharmacology. 36:1781–1791. [PubMed: 21508933]

Rothman, Douglas L.; H, F.; Sibson, Nicolar; Behar, Kevin L.; Mason, Graeme F.; Shen, Jun; Petroff, Ognen AC.; Shulman, Robert G. In Vivo Magnetic Resonance Spectroscopy Studies of The Glutamate and Gaba Neurotransmitter Cycles and Functional Neuroenergetics. Neuropsychopharmacology: The Fifth Generation of Progress. 2002

Fusar-Poli P, Bonoldi I, Yung AR, Borgwardt S, Kempton MJ, Valmaggia L, Barale F, Caverzasi E, McGuire P. Predicting psychosis: meta-analysis of transition outcomes in individuals at high clinical risk. Arch Gen Psychiatry. 2012; 69:220–229. [PubMed: 22393215]

Gaisler-Salomon I, Miller GM, Chuhma N, Lee S, Zhang H, Ghoddoussi F, Lewandowski N, Fairhurst S, Wang Y, Conjard-Duplany A, et al. Glutaminase-Deficient Mice Display Hippocampal Hypoactivity, Insensitivity To Pro-Psychotic Drugs And Potentiated Latent Inhibition: Relevance To Schizophrenia. Neuropsychopharmacology. 2009

Gao XM, Sakai K, Roberts RC, Conley RR, Dean B, Tamminga CA. Ionotropic glutamate receptors and expression of N-methyl-D-aspartate receptor subunits in subregions of human hippocampus: effects of schizophrenia. Am J Psychiatry. 2000; 157:1141–1149. [PubMed: 10873924]

Gonzalez RG, Fischman AJ, Guimaraes AR, Carr CA, Stern CE, Halpern EF, Growdon JH, Rosen BR. Functional MR in the evaluation of dementia: correlation of abnormal dynamic cerebral blood volume measurements with changes in cerebral metabolism on positron emission tomography with fludeoxyglucose F 18. AJNR Am J Neuroradiol. 1995; 16:1763–1770. [PubMed: 8693972]

Gozzi A, Large CH, Schwarz A, Bertani S, Crestan V, Bifone A. Differential Effects of Antipsychotic and Glutamatergic Agents on the phMRI Response to Phencyclidine. Neuropsychopharmacology. 2007

Greene R. Circuit analysis of NMDAR hypofunction in the hippocampus, in vitro, and psychosis of schizophrenia. Hippocampus. 2001; 11:569–577. [PubMed: 11732709]

Harrison PJ. The hippocampus in schizophrenia: a review of the neuropathological evidence and its pathophysiological implications. Psychopharmacology (Berl). 2004; 174:151–162. [PubMed: 15205886]

Heckers S, Konradi C. Hippocampal pathology in schizophrenia. Curr Top Behav Neurosci. 2010; 4:529–553. [PubMed: 21312412]

Heckers S, Rauch SL, Goff D, Savage CR, Schacter DL, Fischman AJ, Alpert NM. Impaired recruitment of the hippocampus during conscious recollection in schizophrenia. Nature Neuroscience. 1998; 1:318–323. [see comment].

Hu Y, Mitchell KM, Albahadily FN, Michaelis EK, Wilson GS. Direct measurement of glutamate release in the brain using a dual enzyme-based electrochemical sensor. Brain Res. 1994; 659:117–125. [PubMed: 7820652]

Imre G, Salomons A, Jongsma M, Fokkema DS, Den Boer JA, Ter Horst GJ. Effects of the mGluR2/3 agonist LY379268 on ketamine-evoked behaviours and neurochemical changes in the dentate gyrus of the rat. Pharmacol Biochem Behav. 2006; 84:392–399. [PubMed: 16857251]

Jentsch JD, Roth RH. The neuropsychopharmacology of phencyclidine: from NMDA receptor hypofunction to the dopamine hypothesis of schizophrenia. Neuropsychopharmacology. 1999; 20:201–225. [PubMed: 10063482]

Kawasaki Y, Suzuki M, Maeda Y, Urata K, Yamaguchi N, Matsuda H, Hisada K, Suzuki M, Takashima T. Regional cerebral blood flow in patients with schizophrenia. A preliminary report. Eur Arch Psychiatry Clin Neurosci. 1992; 241:195–200. [PubMed: 1576174]

Keilhoff G, Becker A, Grecksch G, Wolf G, Bernstein HG. Repeated application of ketamine to rats induces changes in the hippocampal expression of parvalbumin, neuronal nitric oxide synthase and cFOS similar to those found in human schizophrenia. Neuroscience. 2004; 126:591–598. [PubMed: 15183509]

Krystal JH, Abi-Saab W, Perry E, D'Souza DC, Liu N, Gueorguieva R, McDougall L, Hunsberger T, Belger A, Levine L, et al. Preliminary evidence of attenuation of the disruptive effects of the NMDA glutamate receptor antagonist, ketamine, on working memory by pretreatment with the group II metabotropic glutamate receptor agonist, LY354740, in healthy human subjects. Psychopharmacology (Berl). 2005; 179:303–309. [PubMed: 15309376]

Krystal JH, Karper LP, Seibyl JP, Freeman GK, Delaney R, Bremner JD, Heninger GR, Bowers MB Jr, Charney DS. Subanesthetic effects of the noncompetitive NMDA antagonist, ketamine, in humans. Psychotomimetic, perceptual, cognitive, and neuroendocrine responses. Arch Gen Psychiatry. 1994; 51:199–214. [PubMed: 8122957]

Kuhn S, Musso F, Mobascher A, Warbrick T, Winterer G, Gallinat J. Hippocampal subfields predict positive symptoms in schizophrenia: First evidence from brain morphometry. Transl Psychiatry. 2012; 2:e127. [PubMed: 22692142]

Laviola G, Macrì S, Morley-Fletcher S, Adriani W. Risk-taking behavior in adolescent mice: psychobiological determinants and early epigenetic influence. Neuroscience & Biobehavioral Reviews. 2003; 27:19–31. [PubMed: 12732220]

Law AJ, Deakin JF. Asymmetrical reductions of hippocampal NMDAR1 glutamate receptor mRNA in the psychoses. Neuroreport. 2001; 12:2971–2974. [PubMed: 11588613]

Liao Y, Tang J, Corlett PR, Wang X, Yang M, Chen H, Liu T, Chen X, Hao W, Fletcher PC. Reduced dorsal prefrontal gray matter after chronic ketamine use. Biological psychiatry. 2011; 69:42–48. [PubMed: 21035788]

Lin W, Celik A, Paczynski RP. Regional cerebral blood volume: a comparison of the dynamic imaging and the steady state methods. J Magn Reson Imaging. 1999; 9:44–52. [PubMed: 10030649]

Lisman JE, Coyle JT, Green RW, Javitt DC, Benes FM, Heckers S, Grace AA. Circuit-based framework for understanding neurotransmitter and risk gene interactions in schizophrenia. Trends in neurosciences. 2008; 31:234–242. [PubMed: 18395805]

Lorrain DS, Baccei CS, Bristow LJ, Anderson JJ, Varney MA. Effects of ketamine and n-methyl-d-aspartate on glutamate and dopamine release in the rat prefrontal cortex: modulation by a group II selective metabotropic glutamate receptor agonist LY379268. Neuroscience. 2003; 117:697–706. [PubMed: 12617973]

Malaspina D, Harkavy-Friedman J, Corcoran C, Mujica-Parodi L, Printz D, Gorman JM, Van Heertum R. Resting neural activity distinguishes subgroups of schizophrenia patients. Biological psychiatry. 2004; 56:931–937. [PubMed: 15601602]

Malhotra AK, Pinals DA, Adler CM, Elman I, Clifton A, Pickar D, Breier A. Ketamine-induced exacerbation of psychotic symptoms and cognitive impairment in neurolepticfree schizophrenics. Neuropsychopharmacology. 1997; 17:141–150. [PubMed: 9272481]

Medoff DR, Holcomb HH, Lahti AC, Tamminga CA. Probing the human hippocampus using rCBF: contrasts in schizophrenia. Hippocampus. 2001; 11:543–550. [PubMed: 11732707]

Miller TJ, McGlashan TH, Rosen JL, Cadenhead K, Cannon T, Ventura J, McFarlane W, Perkins DO, Pearlson GD, Woods SW. Prodromal assessment with the structured interview for prodromal syndromes and the scale of prodromal symptoms: predictive validity, interrater reliability, and training to reliability. Schizophr Bull. 2003; 29:703–715. [PubMed: 14989408]

Moghaddam B, Adams B, Verma A, Daly D. Activation of glutamatergic neurotransmission by ketamine: a novel step in the pathway from NMDA receptor blockade to dopaminergic and cognitive disruptions associated with the prefrontal cortex. J Neurosci. 1997; 17:2921–2927. [PubMed: 9092613]

Moghaddam B, Adams BW. Reversal of phencyclidine effects by a group II metabotropic glutamate receptor agonist in rats. Science. 1998; 281:1349–1352. [PubMed: 9721099]

Moghaddam B, Javitt D. From revolution to evolution: the glutamate hypothesis of schizophrenia and its implication for treatment. Neuropsychopharmacology. 2012; 37:4–15. [PubMed: 21956446]

Molina V, Reig S, Pascau J, Sanz J, Sarramea F, Gispert JD, Luque R, Benito C, Palomo T, Desco M. Anatomical and functional cerebral variables associated with basal symptoms but not risperidone response in minimally treated schizophrenia. Psychiatry Res. 2003; 124:163–175. [PubMed: 14623068]

Monn JA, Valli MJ, Massey SM, Hansen MM, Kress TJ, Wepsiec JP, Harkness AR, Grutsch JL Jr, Wright RA, Johnson BG, et al. Synthesis, pharmacological characterization, and molecular modeling of heterobicyclic amino acids related to (+)-2-aminobicyclo[3.1.0] hexane-2,6-dicarboxylic acid (LY354740): identification of two new potent, selective, and systemically active agonists for group II metabotropic glutamate receptors. J Med Chem. 1999; 42:1027–1040. [PubMed: 10090786]

Moreno H, Hua F, Brown T, Small S. Longitudinal mapping of mouse cerebral blood volume with MRI. NMR Biomed. 2006; 19:535–543. [PubMed: 16552789]

Moreno H, Wu WE, Lee T, Brickman A, Mayeux R, Brown TR, Small SA. Imaging the abeta-related neurotoxicity of Alzheimer disease. Arch Neurol. 2007; 64:1467–1477. [PubMed: 17923630]

Morey RA, Petty CM, Xu Y, Hayes JP, Wagner HR 2nd, Lewis DV, LaBar KS, Styner M, McCarthy G. A comparison of automated segmentation and manual tracing for quantifying hippocampal and amygdala volumes. Neuroimage. 2009; 45:855–866. [PubMed: 19162198]

Mouri A, Noda Y, Enomoto T, Nabeshima T. Phencyclidine animal models of schizophrenia: approaches from abnormality of glutamatergic neurotransmission and neurodevelopment. Neurochemistry International. 2007; 51:173–184. [PubMed: 17669558]

Narr KL, Thompson PM, Szeszko P, Robinson D, Jang S, Woods RP, Kim S, Hayashi KM, Asunction D, Toga AW, et al. Regional specificity of hippocampal volume reductions in first-episode schizophrenia. Neuroimage. 2004; 21:1563–1575. [PubMed: 15050580]

Paus T, Keshavan M, Giedd JN. Why do many psychiatric disorders emerge during adolescence? Nature Reviews Neuroscience. 2008; 9:947–957.

Paxinos, G.; Franklin, K. The mouse brain in stereotaxic coordinates. 3rd Edition. Amsterdam, Boston: Elsevier Academic Press; 2001.

Pellerin L, Magistretti PJ. Glutamate uptake into astrocytes stimulates aerobic glycolysis: a mechanism coupling neuronal activity to glucose utilization. Proc Natl Acad Sci U S A. 1994; 91:10625–10629. [PubMed: 7938003]

Pinault D. N-methyl d-aspartate receptor antagonists ketamine and MK-801 induce wake-related aberrant gamma oscillations in the rat neocortex. Biological psychiatry. 2008; 63:730–735. [PubMed: 18022604]

Raichle ME. Positron emission tomography. Annu Rev Neurosci. 1983; 6:249–267. [PubMed: 6340590]

Sawiak SJ, Wood NI, Williams GB, Morton AJ, Carpenter TA. Voxel-based morphometry in the R6/2 transgenic mouse reveals differences between genotypes not seen with manual 2D morphometry. Neurobiol Dis. 2009; 33:20–27. [PubMed: 18930824]

Schobel SA, Kelly MA, Corcoran CM, Van Heertum K, Seckinger R, Goetz R, Harkavy-Friedman J, Malaspina D. Anterior hippocampal and orbitofrontal cortical structural brain abnormalities in association with cognitive deficits in schizophrenia. Schizophr Res. 2009a; 114:110–118. [PubMed: 19683896]

Schobel SA, Lewandowski NM, Corcoran CM, Moore H, Brown T, Malaspina D, Small SA. Differential targeting of the CA1 subfield of the hippocampal formation by schizophrenia and related psychotic disorders. Arch Gen Psychiatry. 2009b; 66:938–946. [PubMed: 19736350]

Small SA, Schobel SA, Buxton RB, Witter MP, Barnes CA. A pathophysiological framework of hippocampal dysfunction in ageing and disease. Nat Rev Neurosci. 2011; 12:585–601. [PubMed: 21897434]

Steen RG, Mull C, McClure R, Hamer RM, Lieberman JA. Brain volume in first-episode schizophrenia: systematic review and meta-analysis of magnetic resonance imaging studies. British Journal of Psychiatry. 2006; 188:510–518. [PubMed: 16738340]

Stone JM, Dietrich C, Edden R, Mehta MA, De Simoni S, Reed LJ, Krystal JH, Nutt D, Barker GJ. Ketamine effects on brain GABA and glutamate levels with 1H-MRS: relationship to ketamine-induced psychopathology. Mol Psychiatry. 2012; 17:664–665. [PubMed: 22212598]

Styner M, Gerig G, Lieberman J, Jones D, Weinberger D. Statistical shape analysis of neuroanatomical structures based on medial models. Med Image Anal. 2003; 7:207–220. [PubMed: 12946464]

Styner M, Lieberman JA, Gerig G. Boundary and Medial Shape Analysis of the Hippocampus in Schizophrenia. LNCS. 2003; 2879:464–471.

Vutskits L, Gascon E, Potter G, Tassonyi E, Kiss JZ. Low concentrations of ketamine initiate dendritic atrophy of differentiated GABAergic neurons in culture. Toxicology. 2007; 234:216–226. [PubMed: 17418473]

Yushkevich PA, Piven J, Hazlett HC, Smith RG, Ho S, Gee JC, Gerig G. User-guided 3D active contour segmentation of anatomical structures: significantly improved efficiency and reliability. Neuroimage. 2006; 31:1116–1128. [PubMed: 16545965]

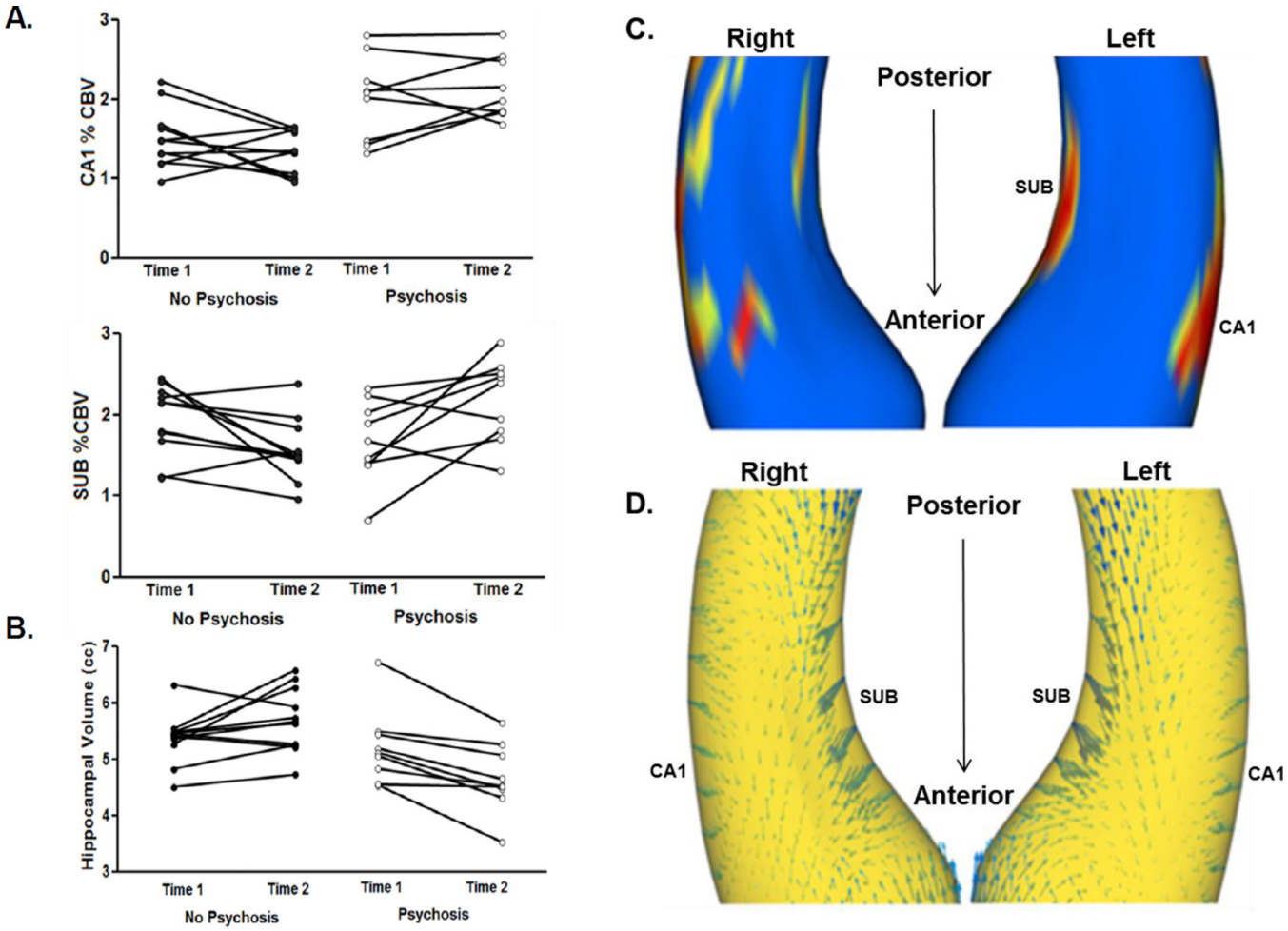

Figure 1. Mapping a spatiotemporal pattern of hippocampal hypermetabolism and atrophy during the emergence of psychosis

(A). Tracking changes in hippocampal cerebral blood volume (%CBV) over time in high-risk subjects who progress to psychosis versus those who do not ('no psychosis') shows that CA1 %CBV (upper graph) is increased in progressors at the pre-psychotic baseline stage ('Time 1') and remains elevated at the onset of psychosis ('Time 2'). In the subiculum (SUB) (lower graph), no %CBV differences were observed at baseline ('Time 1') but an abnormal increase emerged after the onset of psychosis ('Time 2').

(B) No changes in whole hippocampal volume between the progressors ('psychosis') and nonprogressors ('no-psychosis') were observed in the pre-psychotic baseline stage ('Time 1') but atrophy was observed after the onset of psychosis ('Time 2').

(C) Changes in hippocampal morphometric shape over time between the progressors and nonprogressors pinpoints the site of dominant hippocampal volume loss. The right and left hippocampal bodies are shown over the posterior-to-anterior long axis, with warmer colors indicating sites of statistically significant morphometric shape change between the groups over time. A gradient of statistical significance over the long axis is observed, with greatest changes observed in the anterior hippocampal body, in particular in the left CA1 and subiculum.

(D) A vector map shows the directionality of morphometric changes between the groups. Arrows pointing inward along the surface of the hippocampal shape indicate negative hippocampal shape change in progressors to psychosis vs. non progressors, with the greatest

effects observed bilaterally in the anterior CA1 and subiculum. Arrows that run parallel to the long axis, as shown in the anterior uncus and posterior body indicate a shift in three dimensions of the hippocampal body potentially consistent with either shrinkage or movement of the entire structure in space over time between the groups.
See also Tables S1 and S2.

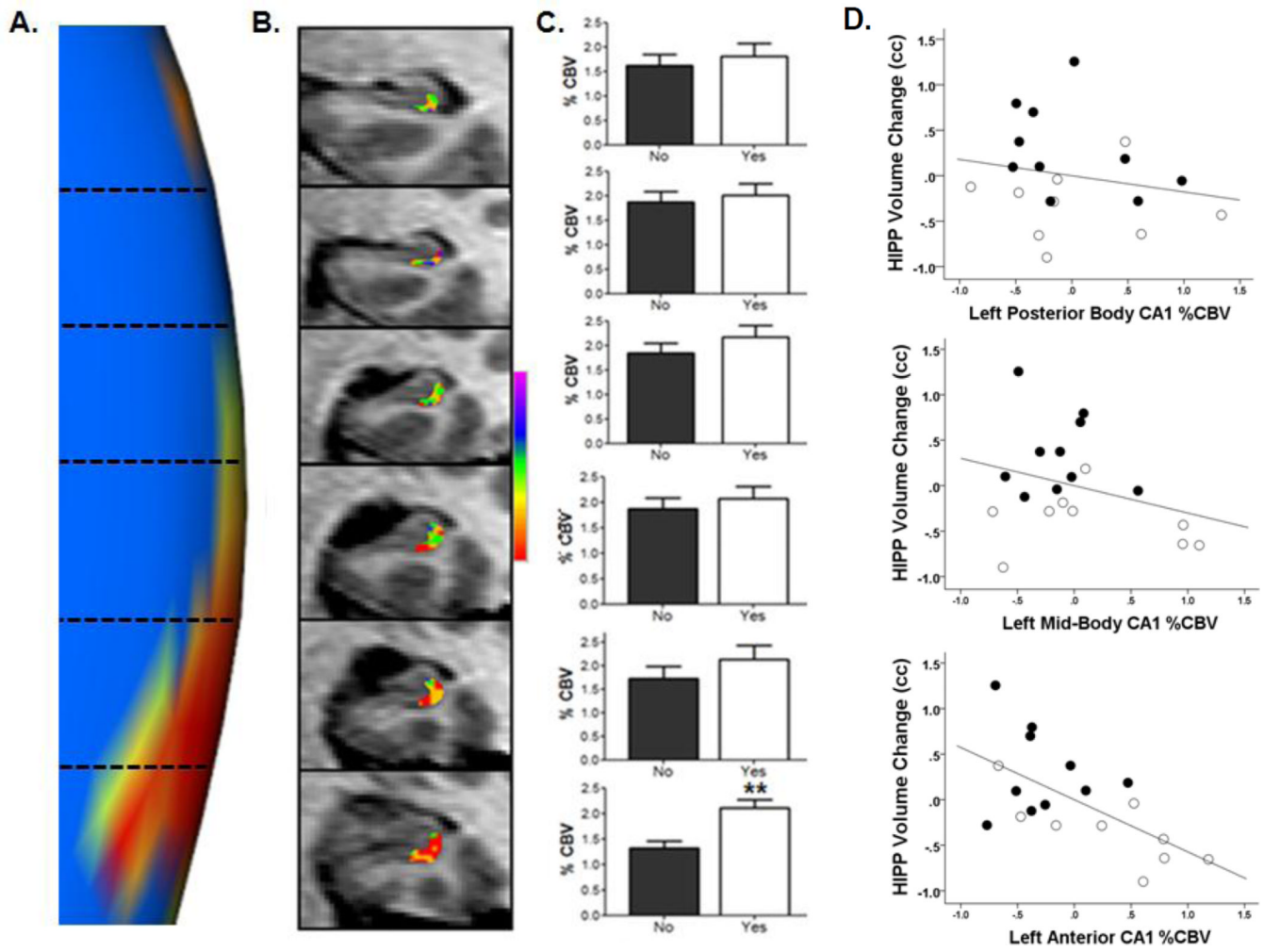

Figure 2. Overlap of anatomical patterns of psychosis-related hypermetabolism and atrophy

(A) Magnified view of Figure 1C, showing the statistical significance p value map of longitudinal left hippocampal body CA1 subfield morphometric shape change between progressors and non-progressors to psychosis. The orientation from posterior (top) to anterior is divided into representative MRI slices along the long-axis of the hippocampal body as indicated by horizontal dotted lines corresponding with frames in Panel B.

(B) Color map of %CBV shown for a single participant acquired at baseline 24 months prior to onset of psychotic symptoms. Illustrated are 3mm slices in the hippocampus body from posterior to anterior of the left CA1 subfield; each frame corresponding with levels demarcated by dotted lines in Panel A. The map shows a gradient in this individual in left CA1, with %CBV progressively higher (warmer colors) in anterior sectors.

(C) Group-wise data of left anterior CA1 %CBV at baseline, showing differences between patients that subsequently progressed to psychosis (progressors; (“yes”, white bars) versus non-progressors (“no”; black bars). Each bar graph corresponds with the posterior-anterior levels demarcated in Panels A and B. **p< 0.01 peak difference in rCBV in progressors relative to non-progressors. Data are represented as mean ± SEM.

(D) The association between baseline left anterior CA1 %CBV and hippocampal (HIPP) volume change. The scatterplots show data averaged from slices 1–6 shown in Panels A–C into two posterior, middle, and anterior slices. There is a negative association between CA1 %CBV and longitudinal hippocampal volume change that becomes progressively stronger

across the posterior-anterior axis reaching significance only in the left anterior CA1 (bottom scatterplot; black=non progressors, white=progressors to psychosis). N=19 of the total n=25 cases are represented in the scatterplot, with n=5 lost to brain imaging follow-up, and one case excluded due to MRI artifact preventing calculation of hippocampal CBV throughout the long axis.
See also Tables S1 and S2.

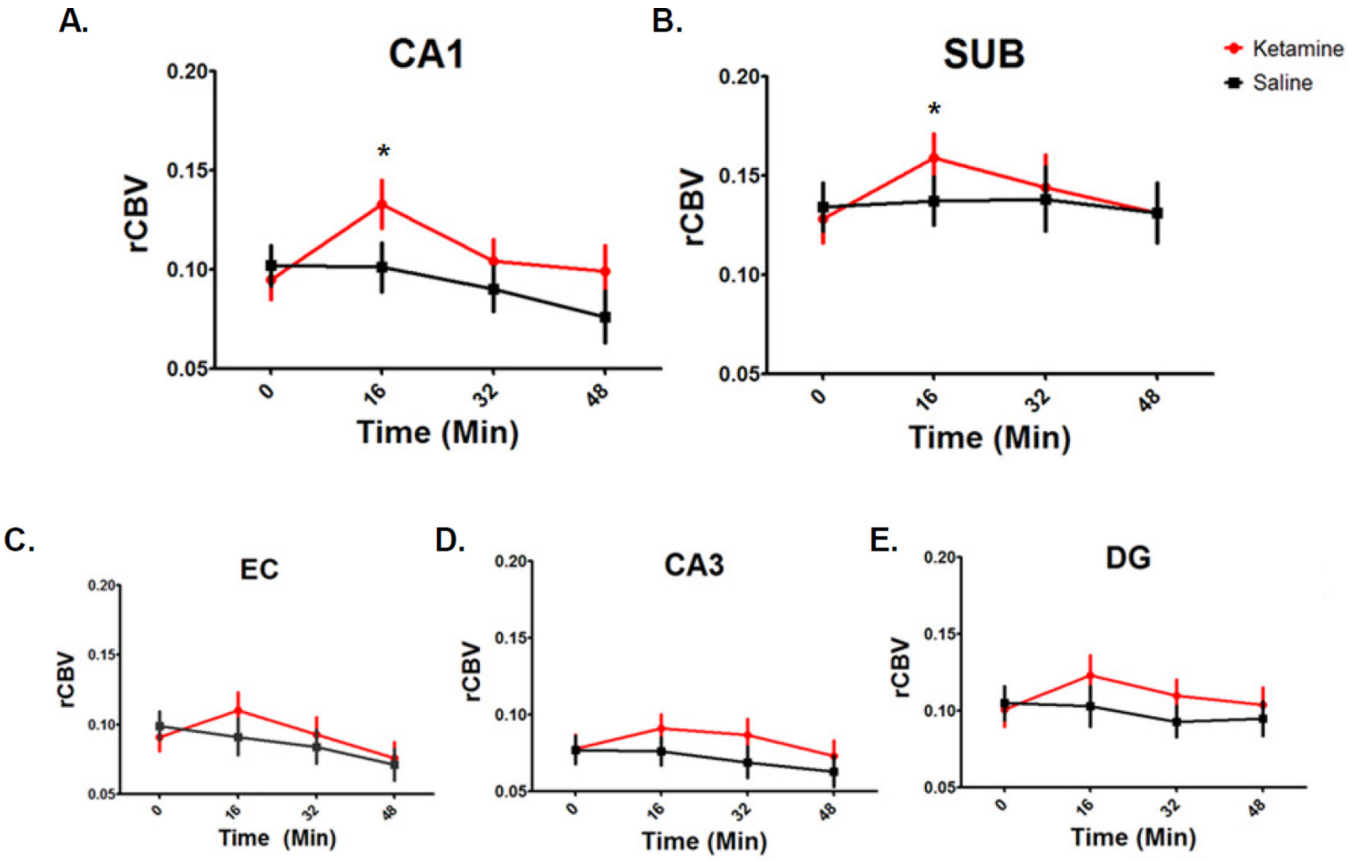

Figure 3. Acute ketamine administration in mice recapitulates the psychosis-associated pattern of hippocampal hypermetabolism

Changes in hippocampal relative CBV (rCBV; see Methods for calculation) in anesthetized mice following acute administration of ketamine (30mg/kg) are shown. Compared to saline (black lines), ketamine (red lines) evoked significant increases in CA1 (Panel A) and subiculum rCBV (Panel B), significant at 16min post injection. The EC (Panel C), CA3 (Panel D), and DG (Panel E) showed non-significant increases relative to saline. *$p < 0.05$ peak difference in rCBV, relative to saline. Data are represented as mean ± SEM.

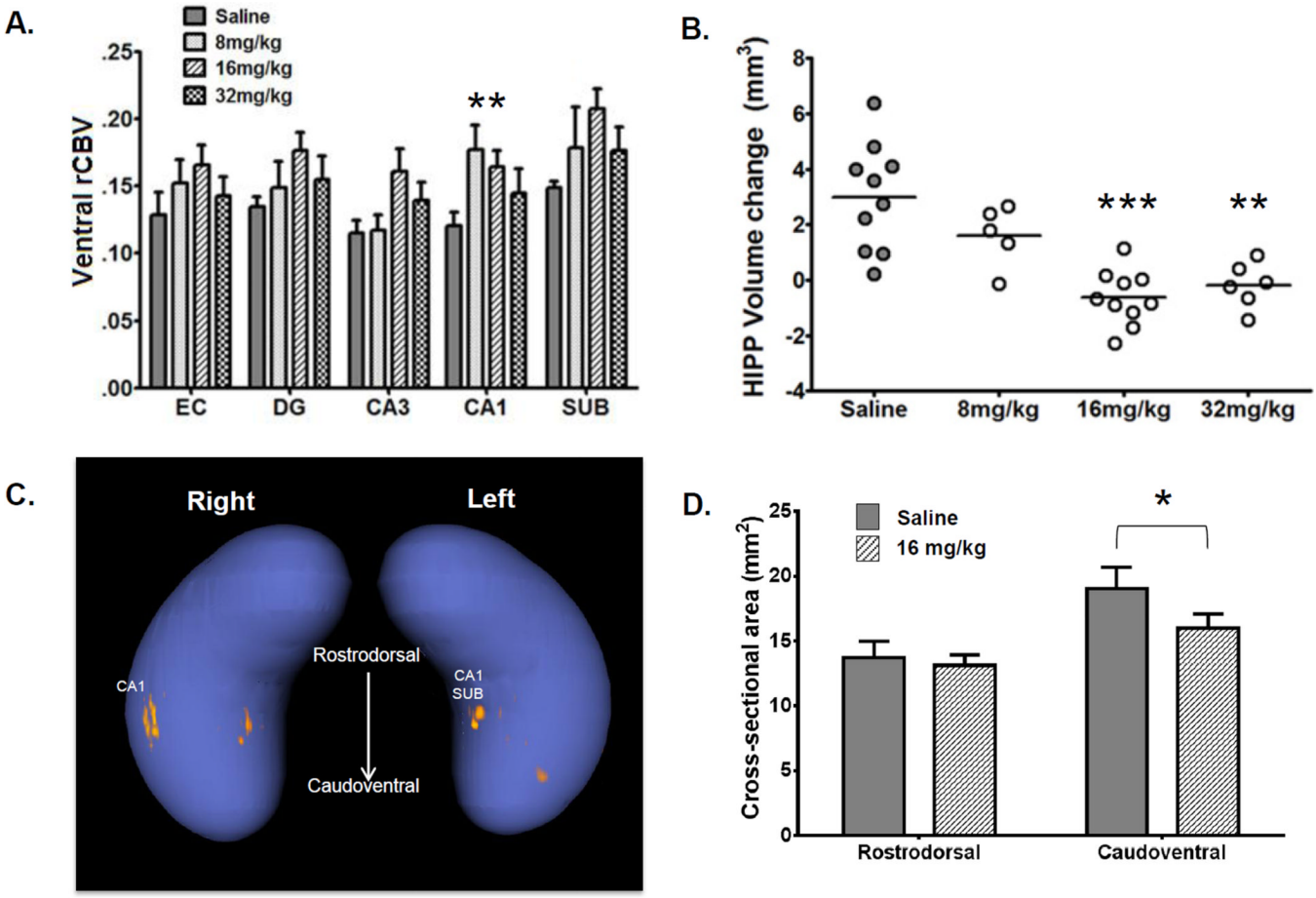

Figure 4. Repeated ketamine administration recapitulates the psychosis-associated pattern of hippocampal hypermetabolism and atrophy

(A) Repeated intermittent ketamine administration over one month (8mg/kg, 16mg/kg, 32mg/kg vs. saline) led to a metabolic state change in hippocampal rCBV: it dose-dependently led to increases in basal rCBV measured at 48 hours after washout of the drug. Statistically significant increases were observed for the 8 and 16 mg/kg repeated treatments. * $p < 0.05$, relative to saline treatment. Data are represented as mean ± SEM.

(B) Compared to saline control, negative hippocampal volume change was found in mice receiving higher doses of repeated ketamine administration, with the effect asymptoting at 16 mg/kg. ** $p < 0.01$; *** $p < 0.01$, relative to saline treatment.

(C) Rostral view of morphometric shape change map. Compared to saline control, areas of negative hippocampal volume change were localized in the 16mg/kg group to the left ventral aspects of hippocampal body by morphometric shape analysis; areas of statistically significant volume loss are shown by orange clusters.

(D) Average cross-sectional hippocampal area (mm^2) as measured in fixed tissue from a subset of mice shown in Panels A–C. Relative to the saline group saline (dark bars), mice receiving repeated ketamine 16 mg/kg (light gray stippled bars) for one month showed areal reductions in the caudoventral aspect of the hippocampus (see main text for anatomical boundaries). * $p < 0.05$ relative to saline. Data are represented as mean ± SEM. See also Figure S1.

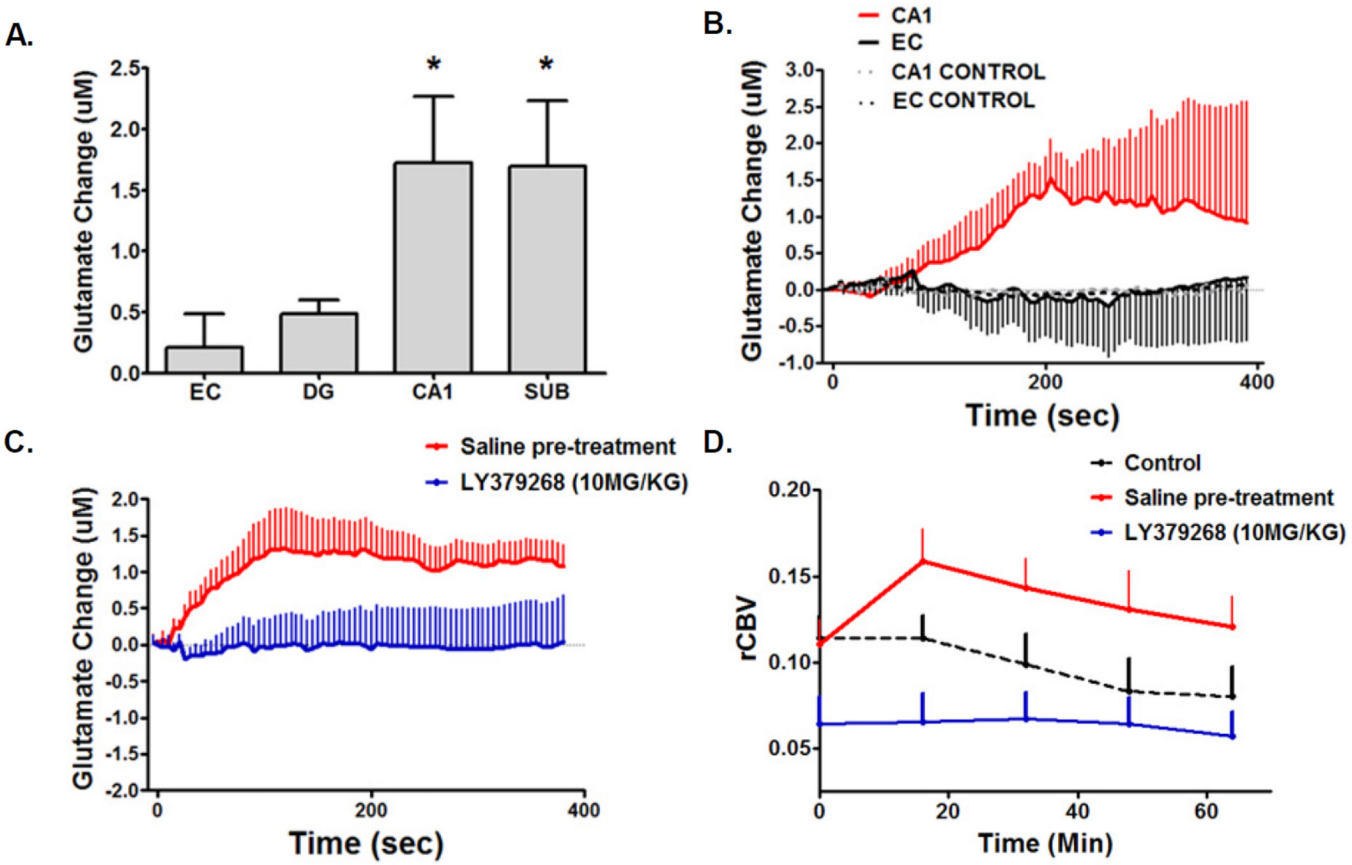

Figure 5. Glutamate mediates the psychosis-associated pattern of hippocampal hypermetabolism induced by acute ketamine administration

(A) As shown by *in vivo* recording of extracellular glutamate efflux performed under the same conditions as for the imaging shown in Figure 3, acute ketamine administration (30mg/kg) resulted in increases in evoked extracellular glutamate in CA1 and subiculum (SUB), and not in entorhinal cortex (EC) or dentate gyrus (DG). * $p < 0.05$ relative to EC.

(B) The time course of the effect of acute ketamine administration in the CA1 (red line) vs. entorhinal cortex (EC; black line).

(C) Pre-treatment with the mGluR2/3 agonist LY379268 (10mg/kg) blocked the evoked extracellular glutamate response within the CA1 subfield.

(D) Relative to saline pre-treatment, pre-treatment with mGluR2/3 agonist LY379268 (10mg/kg) blocked the evoked rCBV response, with a trend for also reducing basal rCBV as measured at “Time 0” (prior to the ketamine challenge).

Data for panels A–D are represented as mean ± SEM. See also Figure S2.

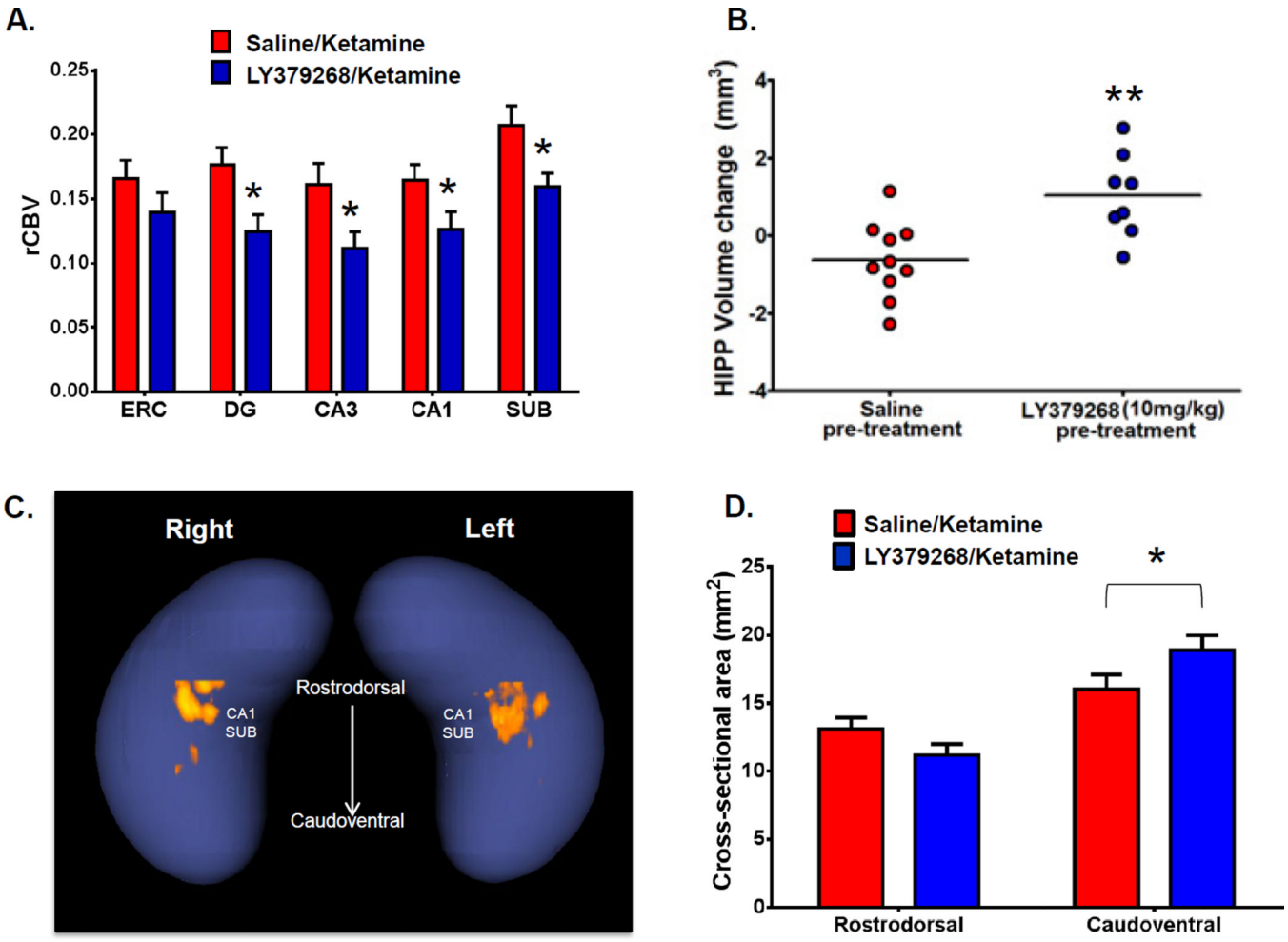

Figure 6. Hippocampal hypermetabolism and volume loss induced by repeated ketamine administration is ameliorated by a glutamate release inhibitor

(A) rCBV following repeated treatment over one month with ketamine and co-treatment with either saline (red bars) or LY379268 10mg/kg (blue bars). Co-treatment with LY379268 ameliorated the repeated ketamine-induced increase in basal hippocampal rCBV, as evident from comparison with saline pretreatment. The saline/ketamine group is the same as that previously shown in Figure 4. * $p < 0.05$ relative to saline.

(B) LY379268 (10mg/kg) co-treatment during repeated ketamine exposure (blue bars) ameliorated the hippocampal (HIPP) volume loss, as evidenced by significantly preserved (larger) HIPP volume in the LY 379268 (blue symbols) relative to the saline co-treatment group (red symbols). ** $p < 0.01$ relative to saline/ketamine.

(C) Rostral view of morphometric shape change map. Pre-treatment with LY379268 resulted in protection in the CA fields of the hippocampal body as measured by MRI-based morphometric analysis; areas of statistically significant volume protection are shown by orange clusters.

(D) Average cross-sectional hippocampal area (mm^2) in fixed brains of mice represented in Panels A–C. Volume protection of LY379268 pre-treatment is most evident in the caudoventral aspect of the hippocampus (see main text for anatomical boundaries). *$p < 0.05$ relative to saline co-treatment ; for all groups, the saline/ketamine group is the same as that represented in Figure 5.

Data for panels A, B, and D are represented as mean ± SEM.

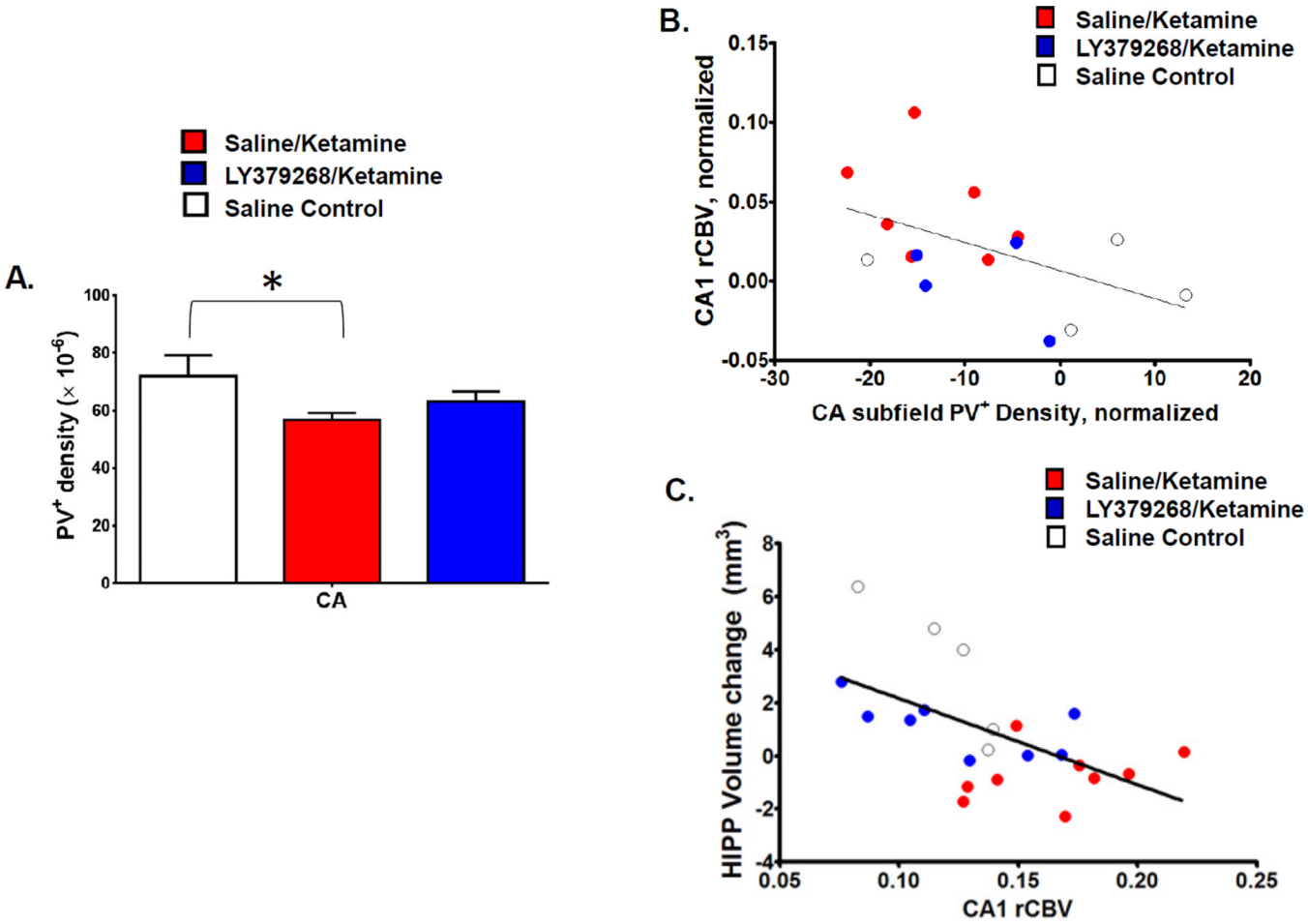

Figure 7. The effects of extracellular glutamate on PV+ interneuron density in the repeated ketamine exposure model

(A) Intermittent repeated ketamine exposure resulted in a decrease in the apparent density of PV+ interneurons in hippocampal CA subfields; this effect is attenuated by LY379268 co-treatment. ** $p < 0.01$ Saline/Ketamine group versus saline control. Data are represented as mean ± SEM.

(B) Decreases in PV+ expression (relative the mean of the saline control group) are associated at trend level with increases in basal rCBV measured after one month of repeated treatment with saline only (open symbols), ketamine with saline co-treatment (red symbols) or ketamine with LY379268 co-treatment (blue symbols) (r=.49, p=.06).

(C) Across the same treatment groups there is a negative association between post-treatment basal rCBV measured after drug wash-out and the change in hippocampal volumes across the 1-month treatment period (r=.57, p=.006).